REPORT No. 288

PRESSURE DISTRIBUTION OVER A RECTANGULAR MONOPLANE WING MODEL UP TO 90° ANGLE OF ATTACK

By MONTGOMERY KNIGHT and OSCAR LOESER, Jr.
Langley Memorial Aeronautical Laboratory

REPORT No. 288

PRESSURE DISTRIBUTION OVER A RECTANGULAR MONOPLANE WING MODEL UP TO 90° ANGLE OF ATTACK

By Montgomery Knight and Oscar Loeser, Jr.

SUMMARY

The pressure distribution tests herein described, covering angles of attack up to 90°, were made on a rectangular monoplane wing model in the atmospheric wind tunnel of the Langley Memorial Aeronautical Laboratory.

These tests indicate that a rectangular wing, by reason of its large tip loads, is uneconomical aerodynamically and structurally, has pronounced lateral instability above maximum lift, and is not adaptable to accurate calculation based on the classical wing theory.

INTRODUCTION

The pressure distribution tests described in this report were made at the Langley Memorial Aeronautical Laboratory primarily to obtain information relative to the autorotational characteristics of a particular rectangular monoplane wing model. However, the results obtained are indicative of the distribution over square-tipped monoplane wings in general, and are presented herewith at the suggestion of Lieut. W. S. Diehl, United States Navy, to add to the meager supply of information on the aerodynamic characteristics of wings at large angles of attack. Such information is of value in studies of the spinning airplane and of stability and controllability at large angles of attack.

METHODS AND APPARATUS

The tests, covering angles of attack (α) from $-8°$ (approximately zero lift) to 90°, were made in the 5-foot atmospheric wind tunnel, which has a circular closed throat. (Reference 1.) The method of half-span wing and reflecting plane (references 2, 3, 4, 5) was used. In Figure 1 is shown the arrangement of wing and plane in the tunnel. Retardation of the flow close to the plane is compensated for by dipping the leading edge of the plane slightly, the correct amount of dip being determined from a series of velocity surveys taken normal to the plane.

The rectangular mahogany wing which had a Göttingen 387–FB (flat bottom) profile, had been tested previously in autorotation experiments as a 5-inch by 30-inch full-span wing. For pressure distribution purposes, 12 small brass tubes were inlaid in slots cut in the surface of the wing parallel to the span. The pressure orifices consisted of holes drilled at intervals in these tubes. The tube locations around the profile, and the spacing of orifice groups or sections along the span, are given in Figure 2. Figure 3 shows the model with tubes, connections, and mounting block.

Pressures were recorded photographically on photostat paper placed against the tubes in the multiple liquid manometer illustrated in Figure 4. In this figure are also shown the rubber pressure tubes from the wing, and the handles attached to the lower end of the wing supporting bracket for changing the angle of attack.

In order to simplify the drawing of the pressure distribution diagrams, the positions of the orifice tubes in the wing surface were so chosen that when projected on the chord they corresponded to certain selected tubes on the manometer, the distance between the end manometer tubes representing the wing chord. This arrangement made it possible to draw the pressure diagrams directly on the manometer record as shown in Figure 5, which is a photograph of a specimen record. Only the manometer tubes labeled at the top of this record were used in the tests, the others being left open to the air in the experimental chamber.

The testing procedure consisted first in sealing all orifices with wax, checking each tube for leaks, and then opening with a needle the orifices of the desired section. This section was then tested through the complete angle of attack range.

Throughout the tests the dynamic pressure ($q = \frac{1}{2} \rho V^2$, where ρ = air density and V = velocity) in the vicinity of the model was held constant at 4.09 pounds per square foot, using as

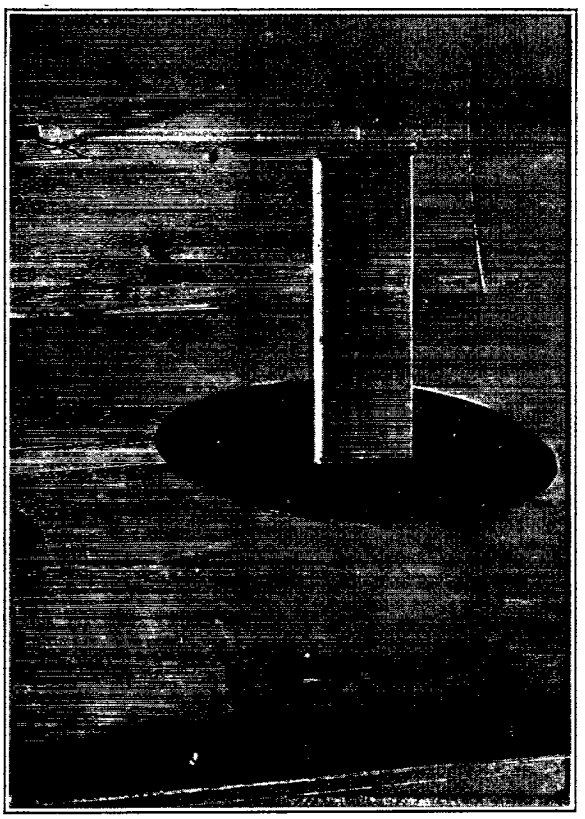

FIG. 1.—Half-span wing model and reflecting plane mounted in tunnel

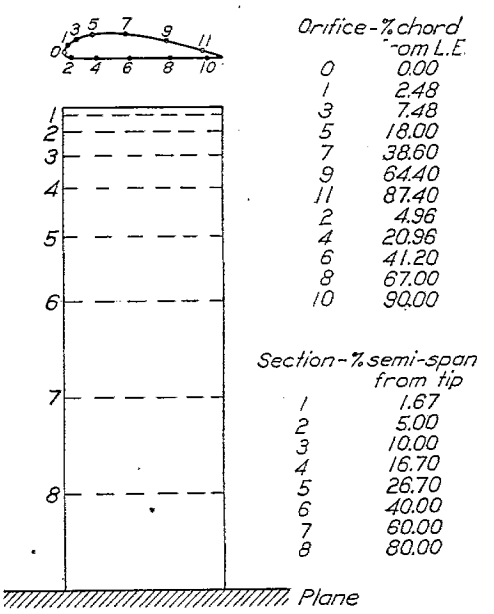

FIG. 2.—Location of pressure distribution orifices in Göttingen 387-FB wing

a reference the Pitot-static tube shown at the left of Figure 1. This instrument was connected to a vernier manometer outside the tunnel. The static pressure side of this Pitot tube was also connected to two of the multiple manometer tubes for the purpose of locating the static pressure line on the manometer record. The mean velocity corresponding to the above dynamic pressure was 59.5 feet per second. The mean Reynolds Number was 147,000, with the wing chord as the characteristic length.

A comparison of the integrated areas of original and check manometer records indicated over-all errors of about 1 per cent, covering the tests and the drawing and integration of the pressure diagrams. This error, together with the error in the values of q used in computing the coefficient of normal force (C_{NF}) for each section, resulted in a probable error of about 3 per cent in the final results.

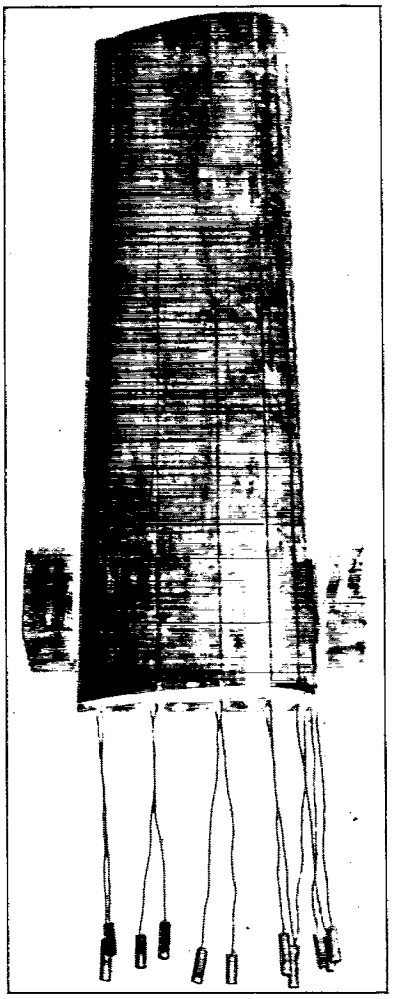

FIG. 3.—Model wing showing pressure connections and mounting block

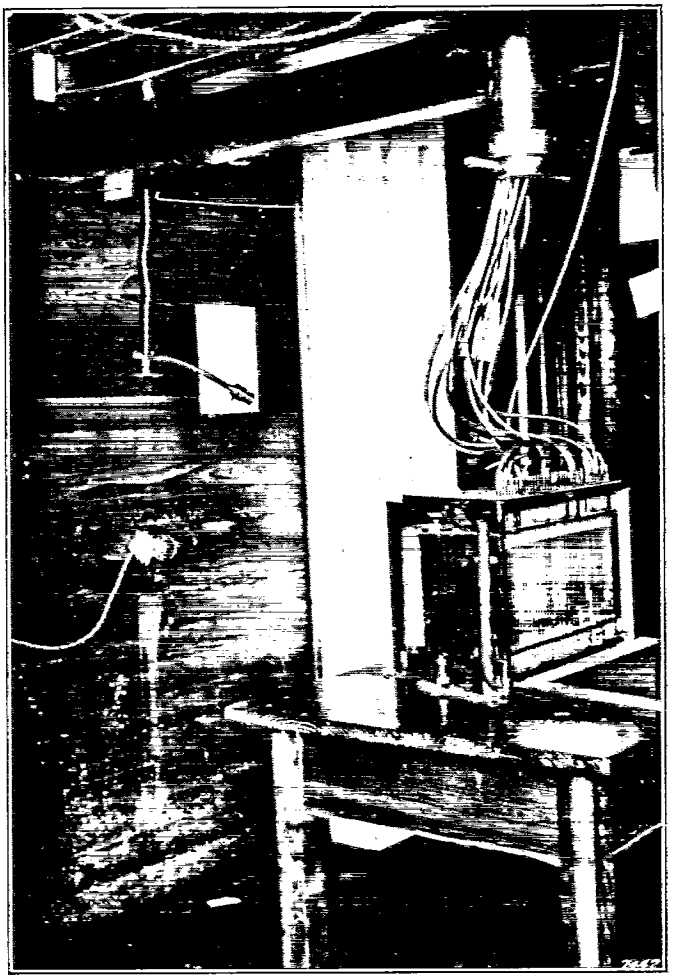

FIG. 4.—Multiple photographic manometer in place beneath tunnel

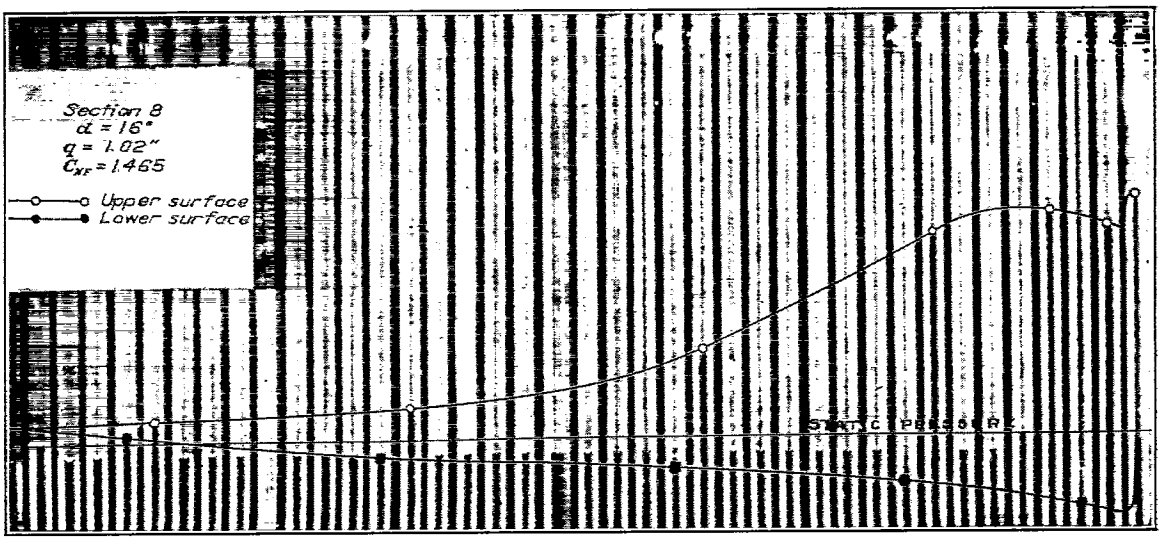

FIG. 5.—Specimen manometer record with pressure diagram

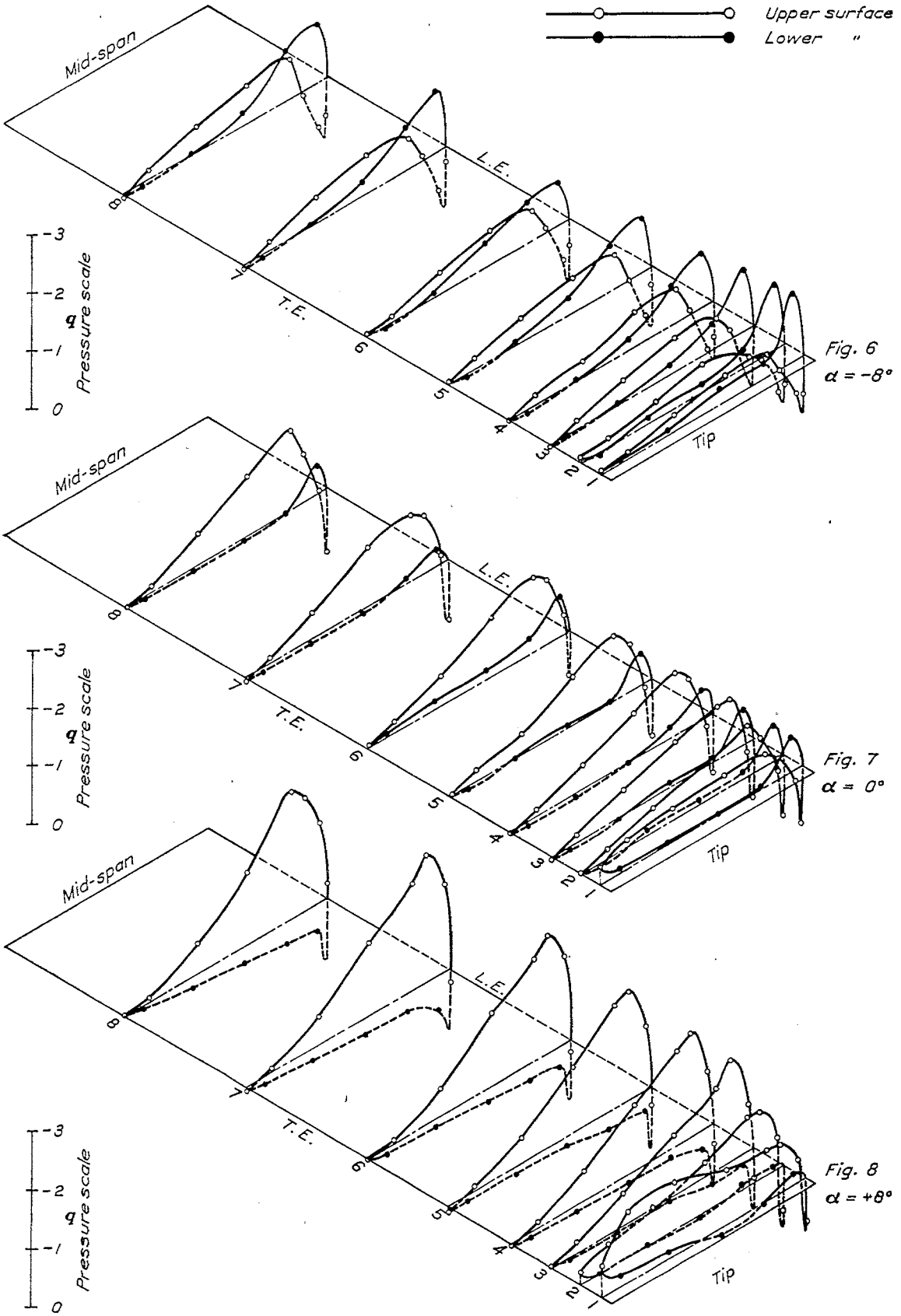

Fig. 6
$\alpha = -8°$

Fig. 7
$\alpha = 0°$

Fig. 8
$\alpha = +8°$

FIGS. 6, 7, and 8.—Surface normal pressure distribution

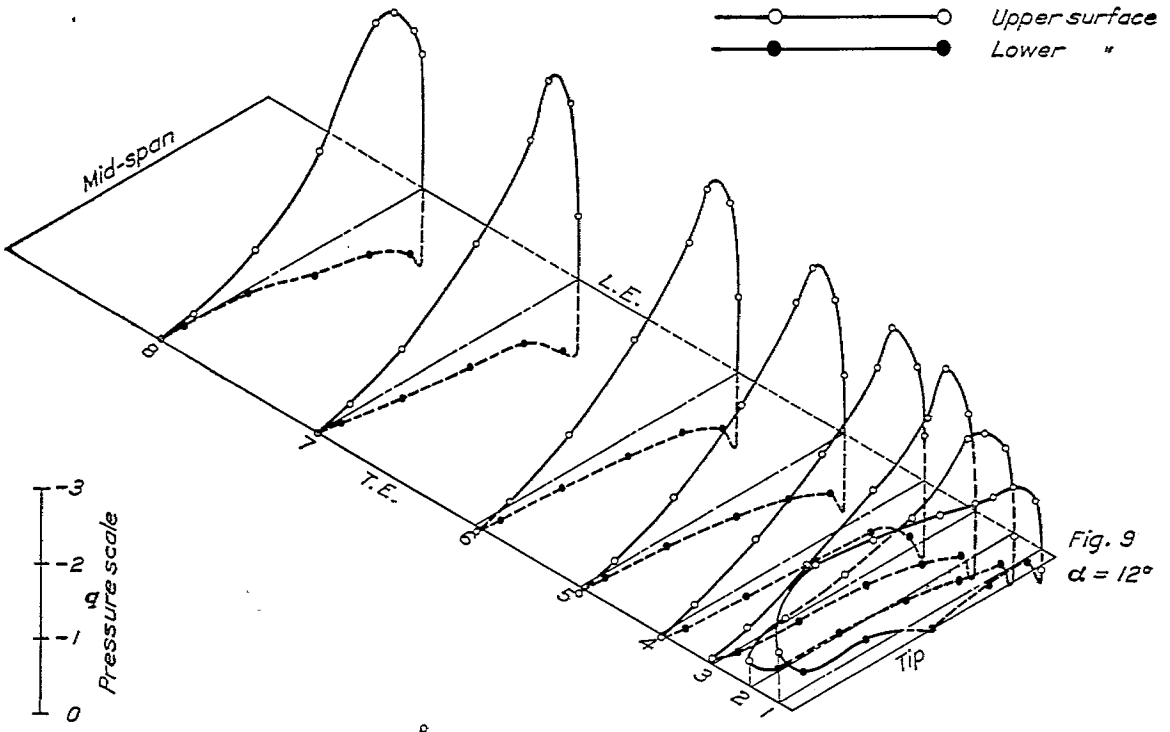

Fig. 9
$\alpha = 12°$

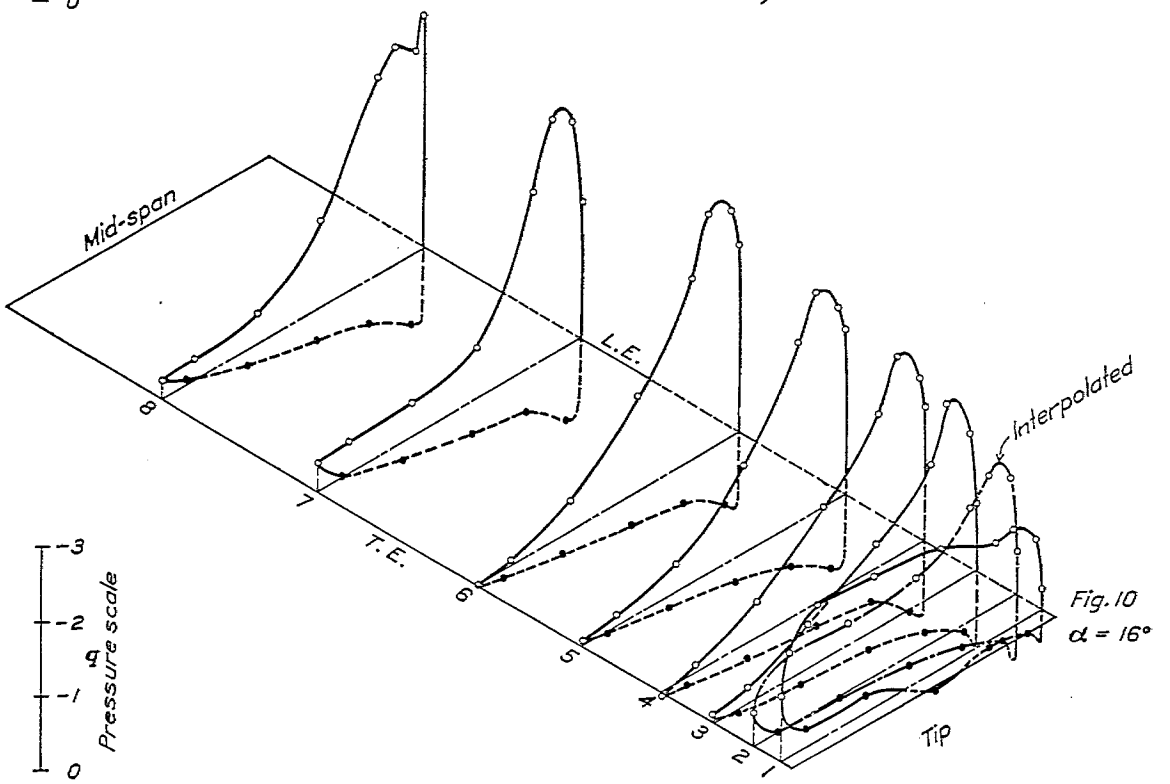

Fig. 10
$\alpha = 16°$

FIGS. 9 and 10.—Surface normal pressure distribution

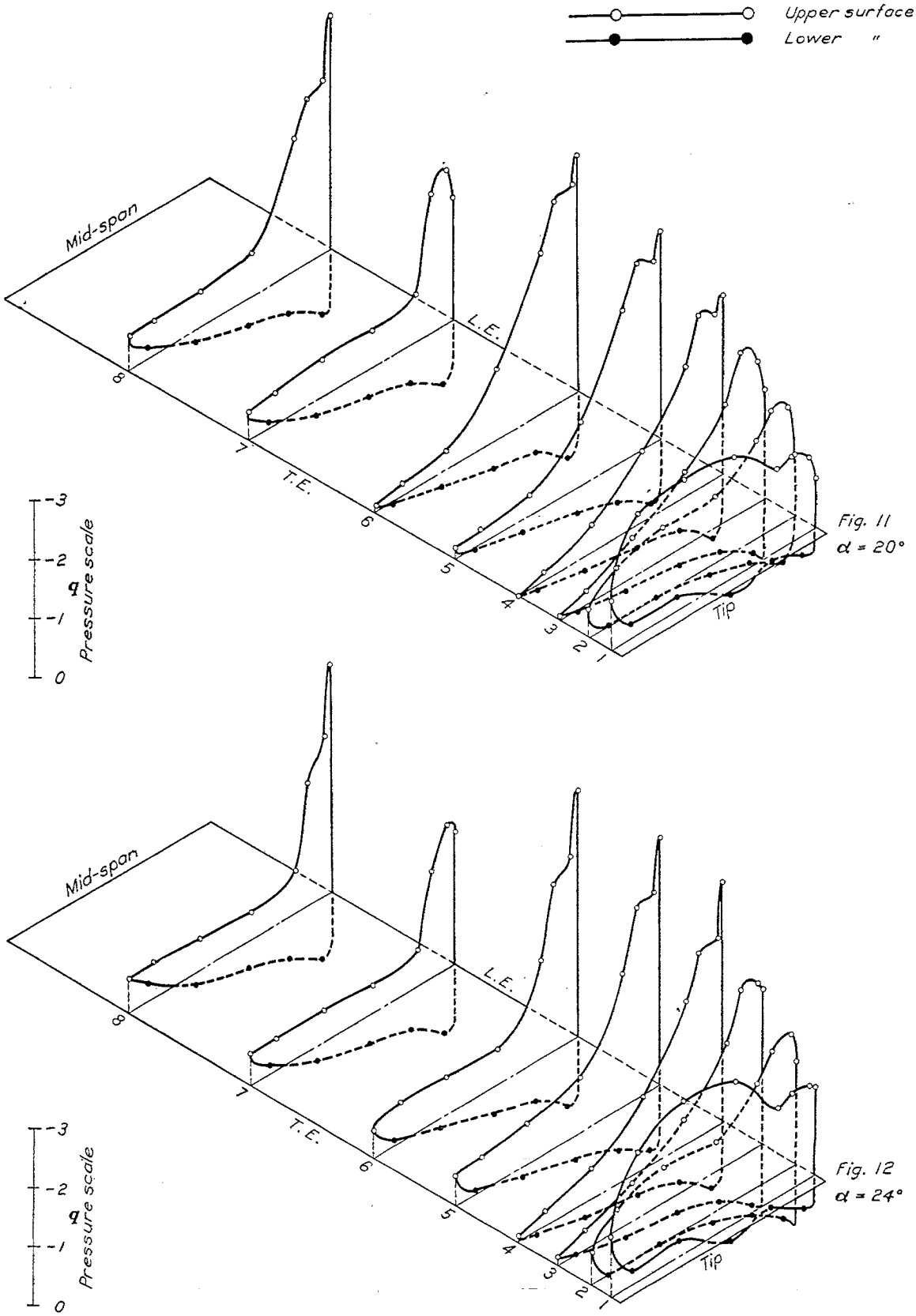

Fig. 11
$\alpha = 20°$

Fig. 12
$\alpha = 24°$

FIGS. 11 and 12.—Surface normal pressure distribution

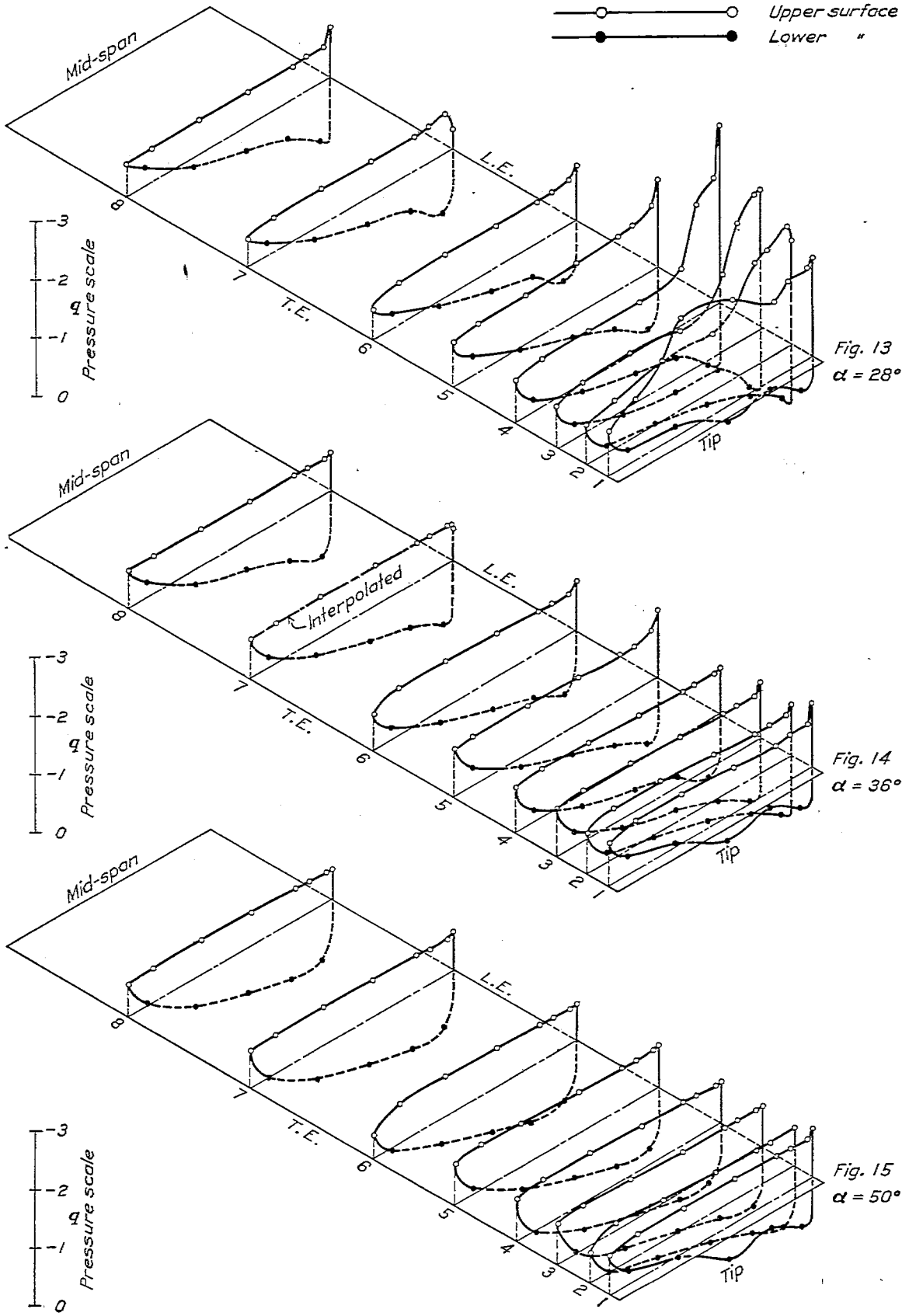

FIGS. 13, 14, and 15.—Surface normal pressure distribution

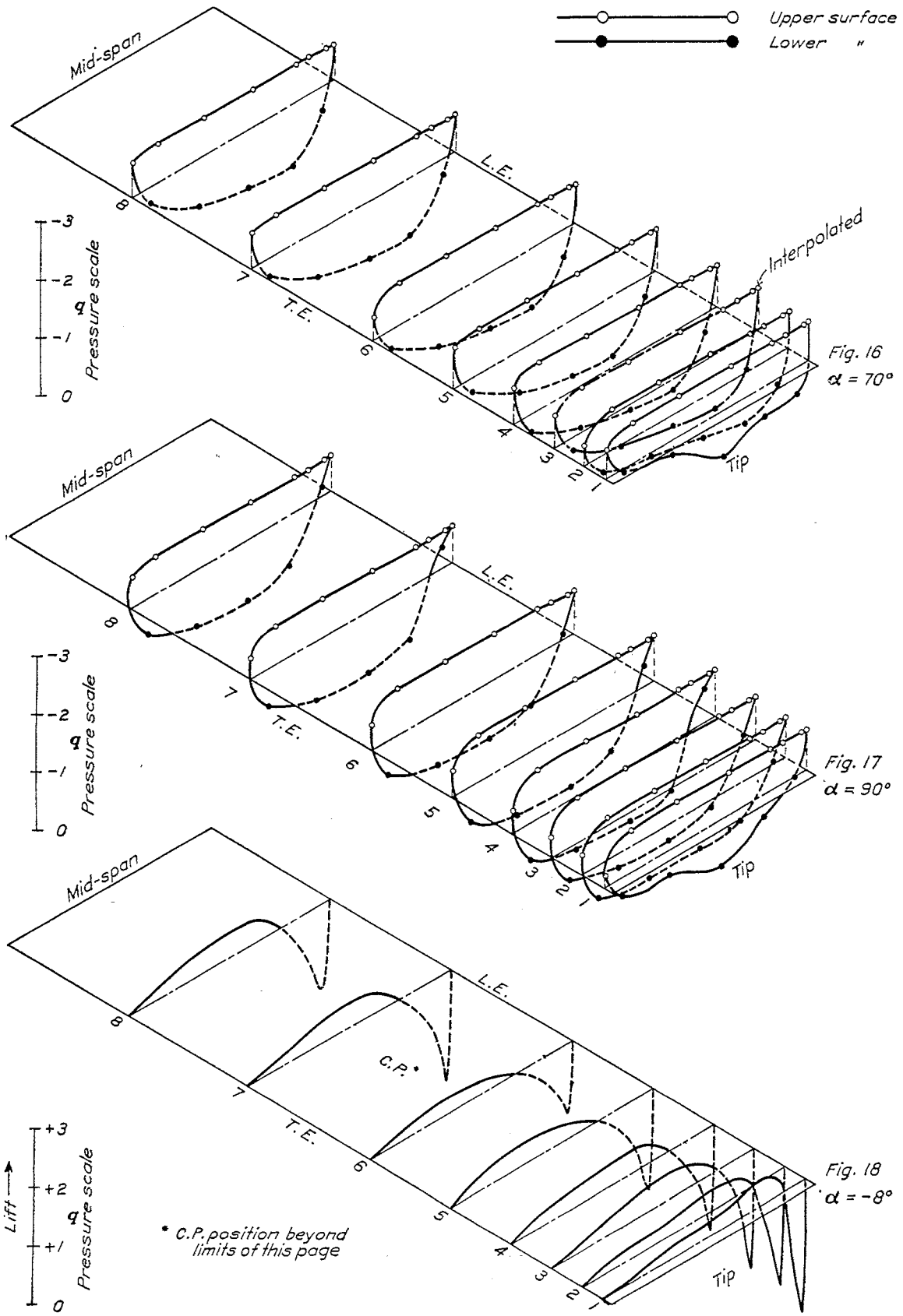

FIGS. 16 and 17.—Surface normal pressure distribution
FIG. 18.—Resultant normal pressure distribution

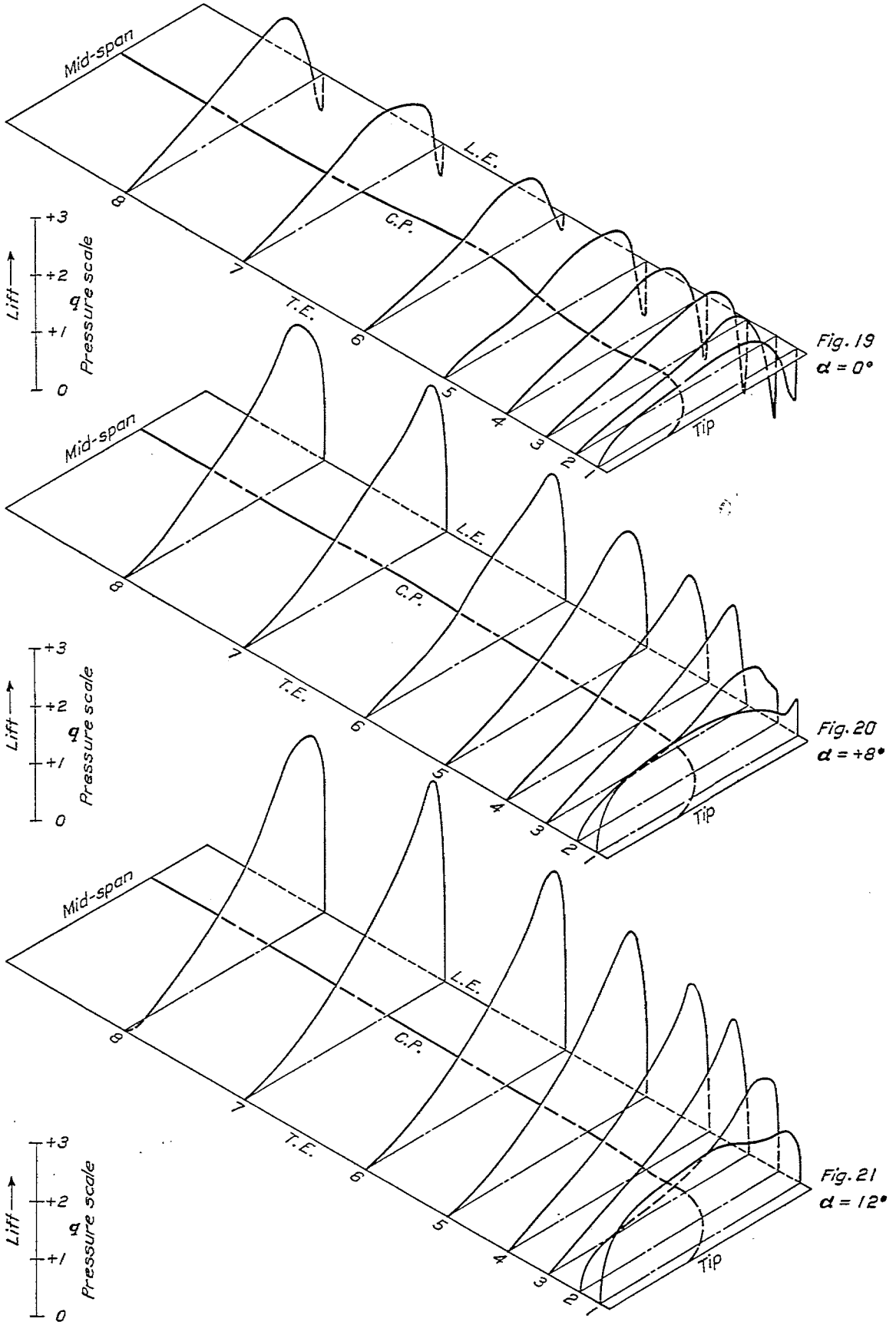

FIGS. 19, 20, and 21.—Resultant normal pressure distribution

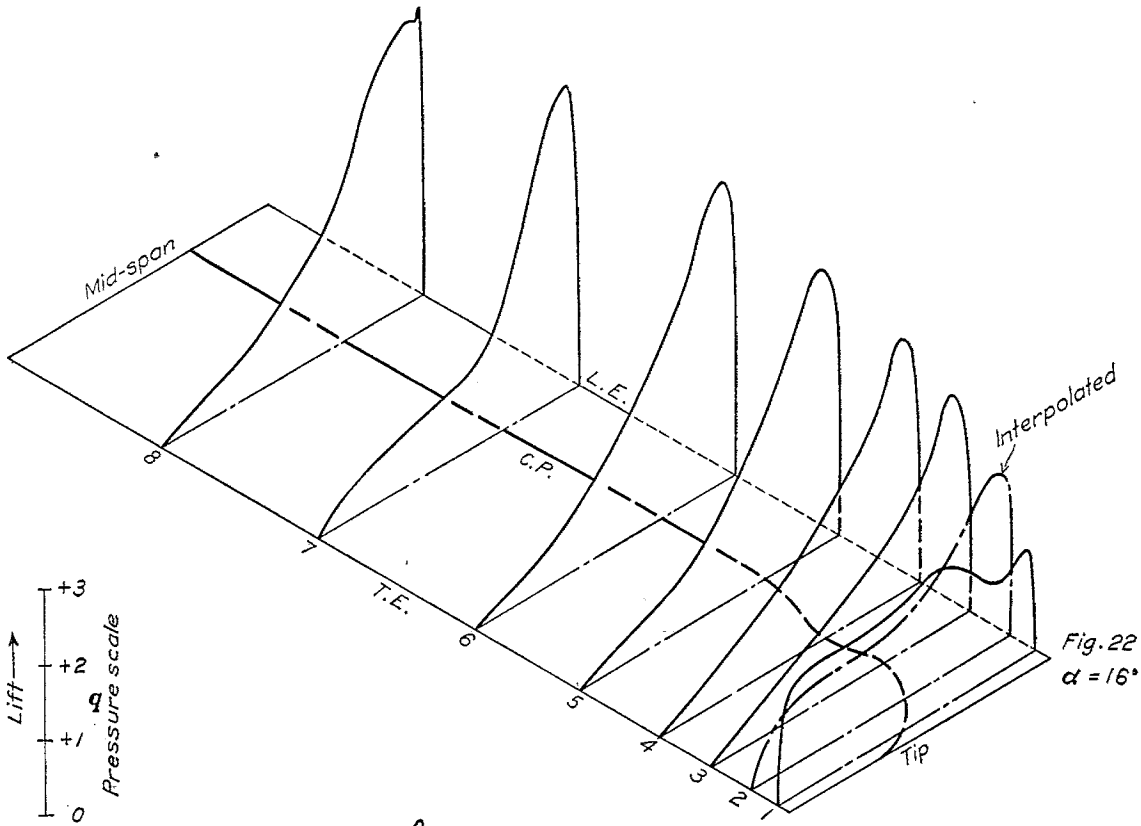

Fig. 22
$\alpha = 16°$

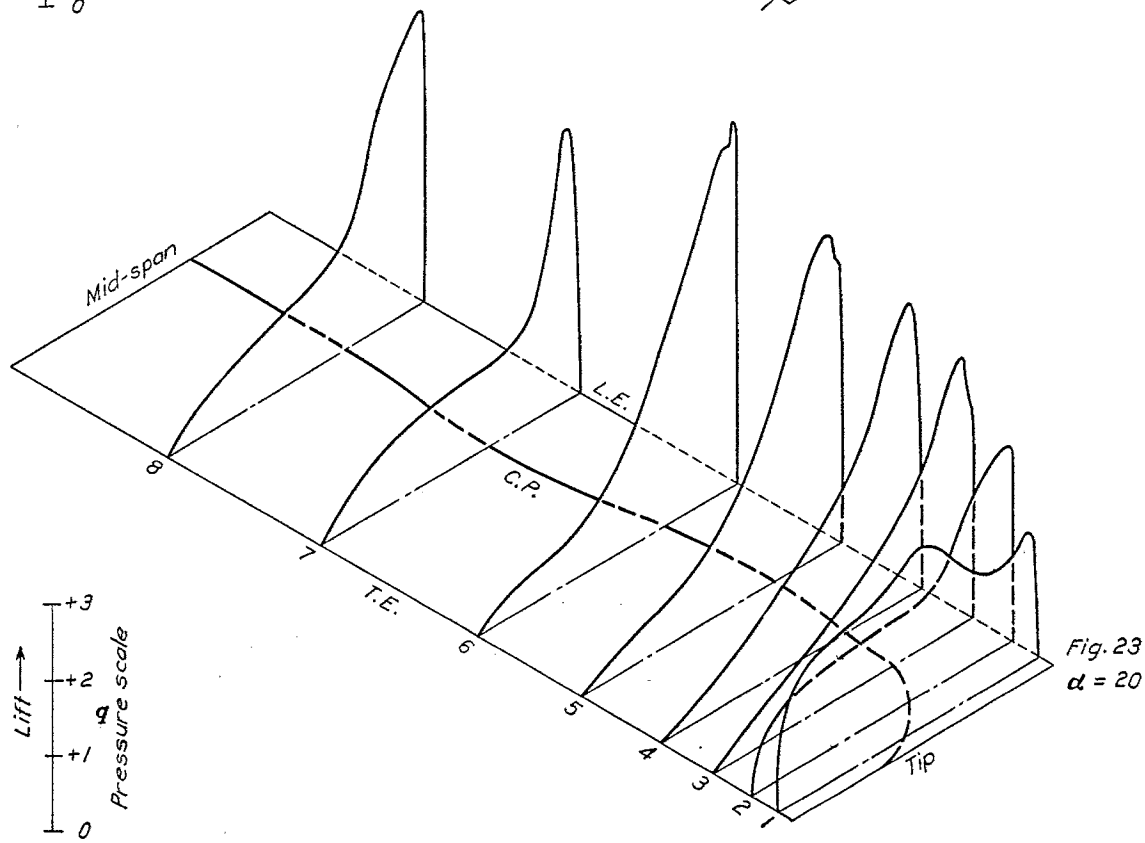

Fig. 23
$\alpha = 20°$

FIGS. 22 and 23.—Resultant normal pressure distribution

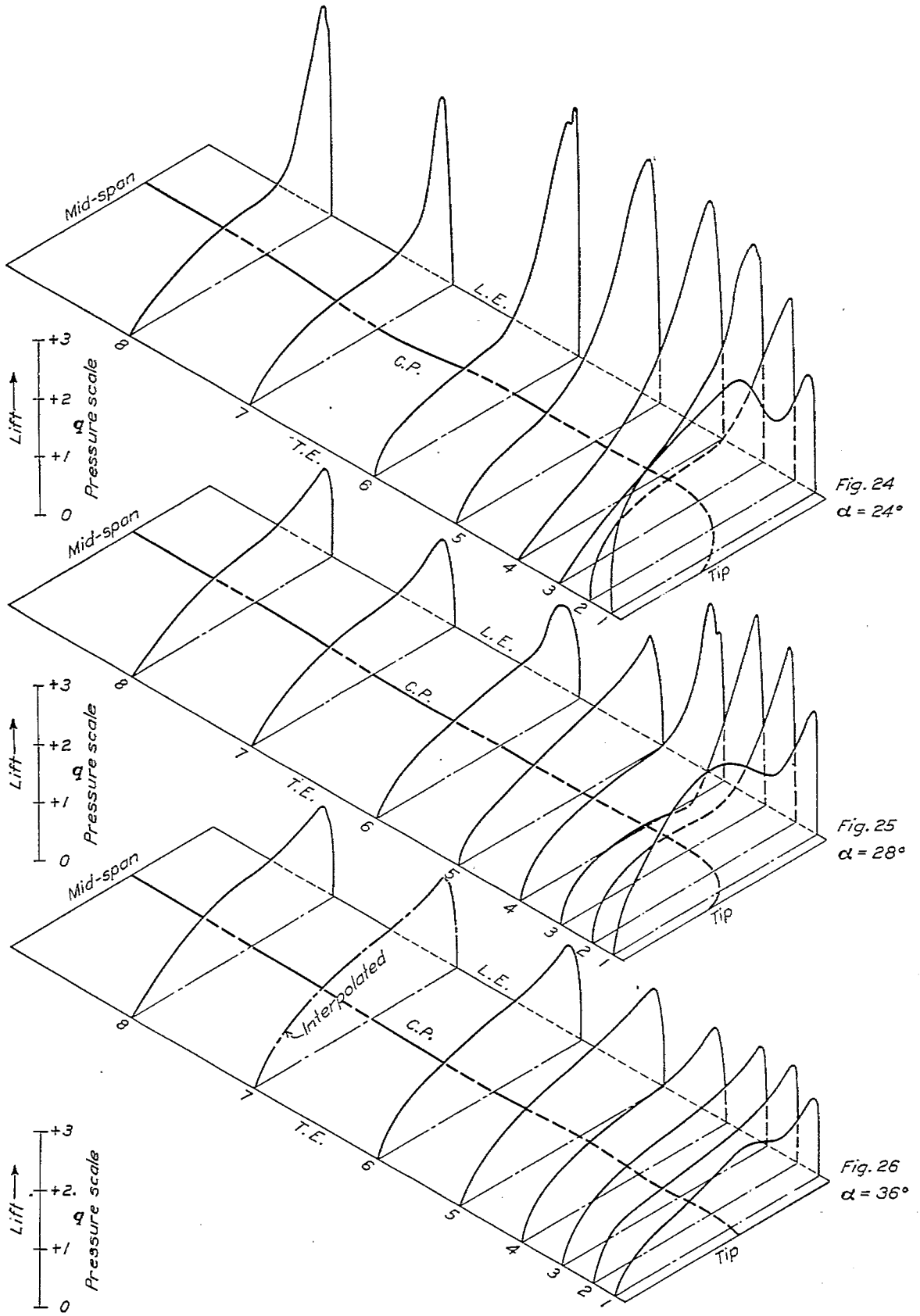

FIGS. 24, 25, and 26.—Resultant normal pressure distribution

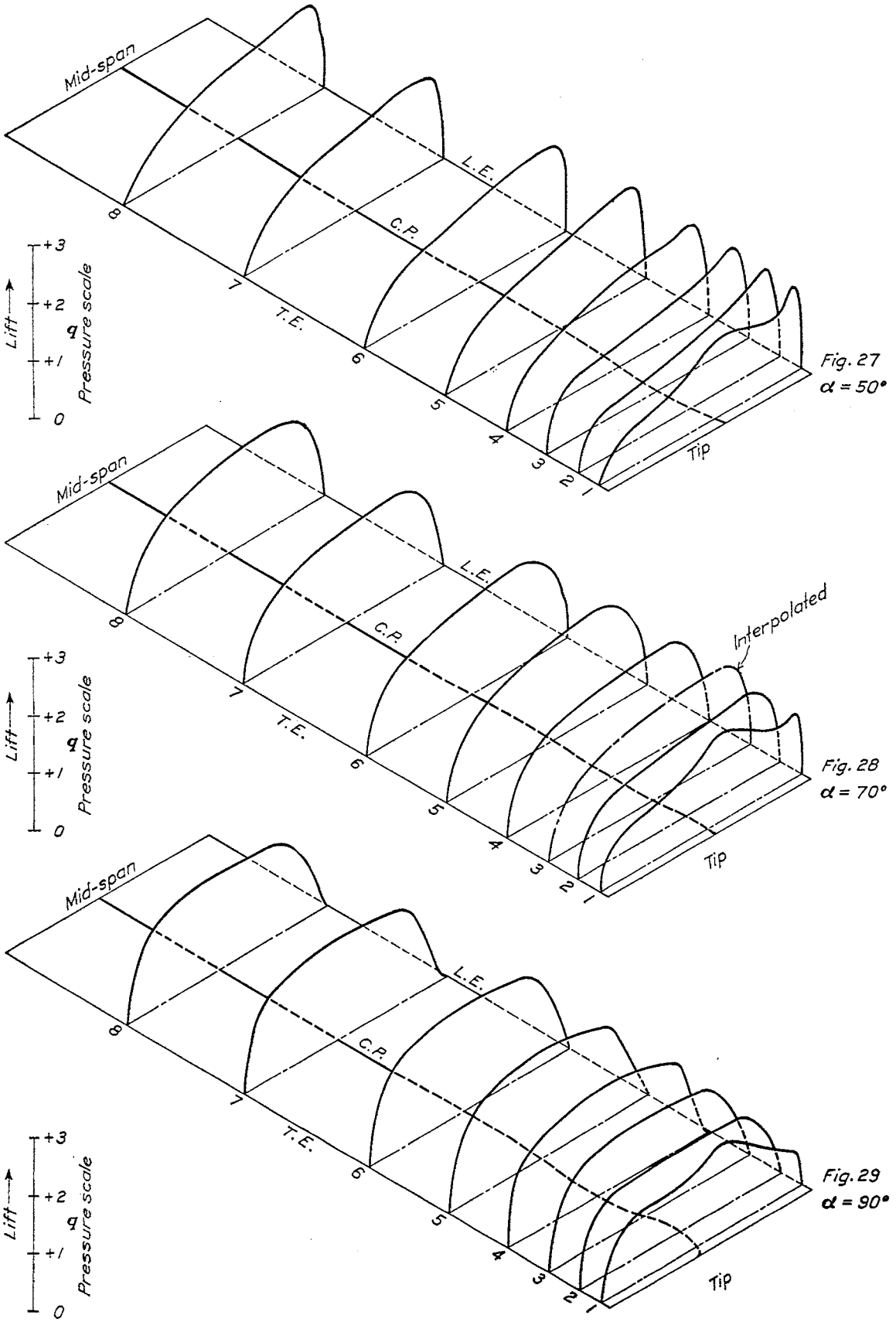

FIGS. 27, 28, and 29.—Resultant normal pressure distribution

RESULTS

In order to give a three-dimensional impression of the distribution of pressure over the wing model, the pressure diagrams for each section at a given angle of attack are plotted in their respective positions along the span of an isometric plan view of the half wing. The pressures on the upper and lower wing surfaces are presented in this manner in Figures 6–17. Negative

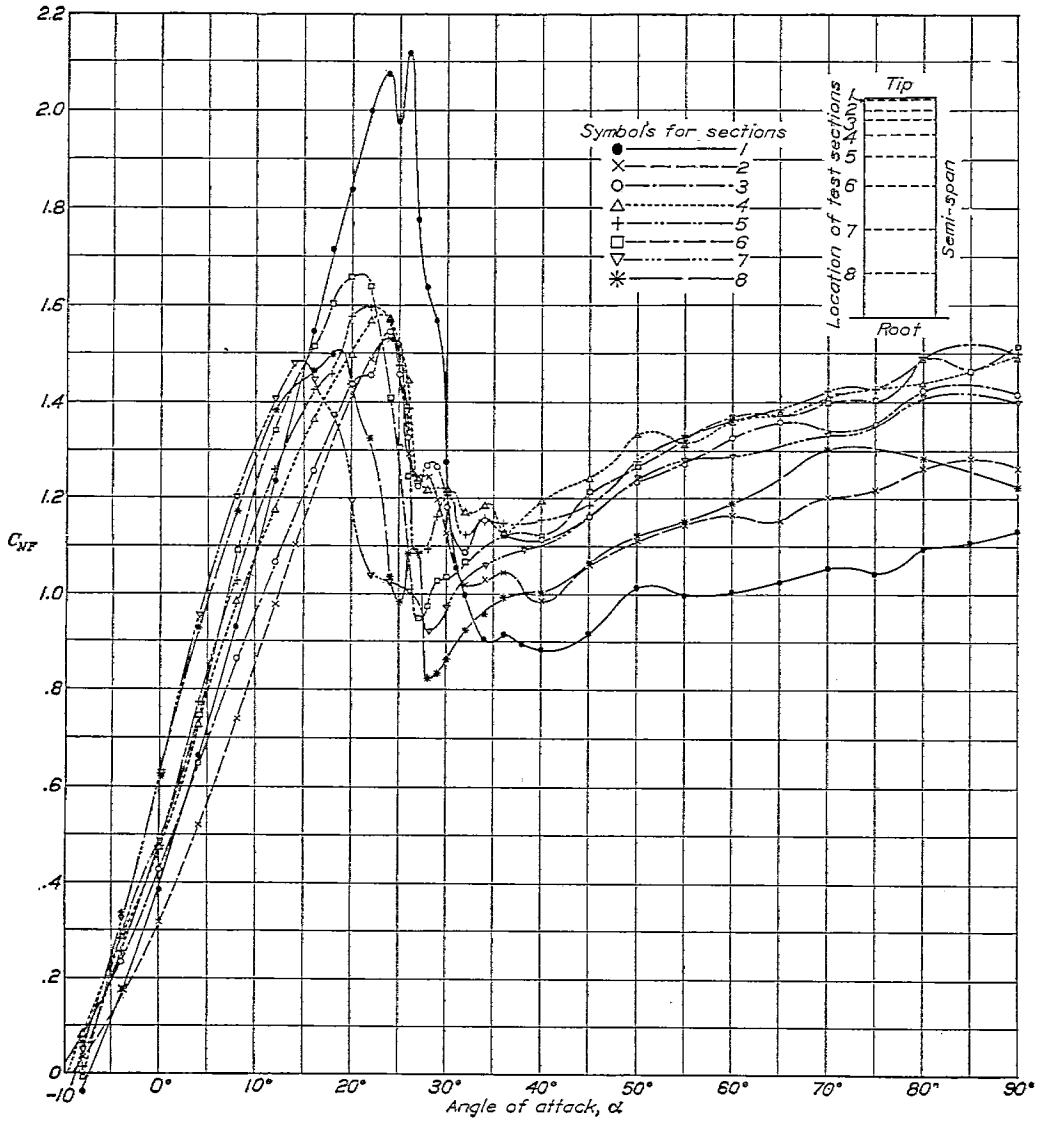

FIG. 30.—Section curves of C_{NF}

pressures are plotted upward and positive pressures downward with respect to the chord plane. Figures 18–29 are corresponding diagrams of resultant or total pressures. Lifting pressures are plotted upward. The latter diagrams also contain curves of centers of pressure (C. P.) along the span. A pressure scale in terms of q is included at the left of each figure. Each of the two sets of diagrams is for angles of attack of $-8°$, 0, 8°, 12°, 16°, 20°, 24°, 28°, 36°, 50°, 70°, and 90°, the angles being so chosen that interpolations may be made with fair accuracy.

In Figure 30 are given the curves of C_{NF} vs. α for each section. The values of C_{NF} were obtained directly from the manometer records by integrating the pressure diagrams—

$$C_{NF}=\frac{A}{ql}$$

where A = integrated area of diagram,

q = dynamic pressure expressed as pressure head determined from stagnation point,

l = length of diagram.

The determination of q at large angles of attack proved to be a difficult matter. From a careful study of the stagnation points of the pressure diagrams a curve of q vs. α was finally obtained for each section. The values of q taken from these curves were used in the above equation for C_{NF}.

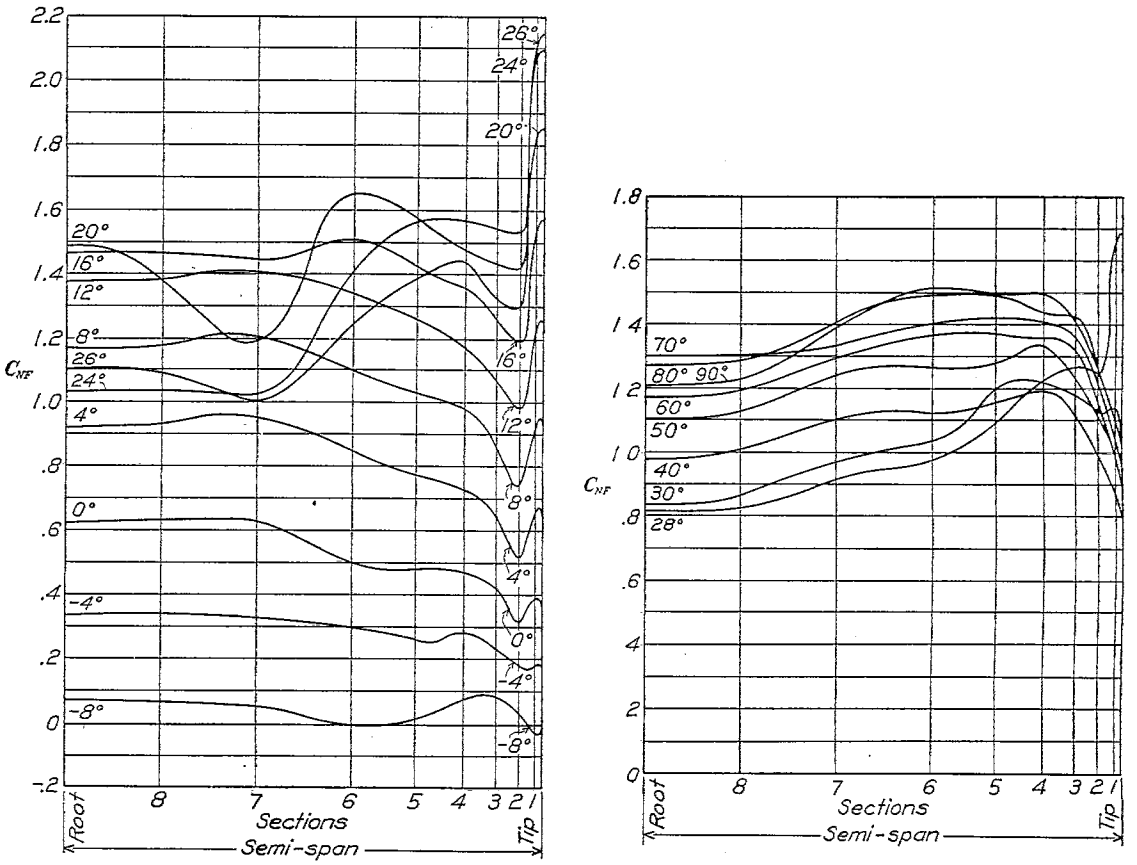

FIGS. 31a and 31b.—Semispan loads

Considering the wing as a "lifting line," C_{NF} is merely the pressure in terms of q at any point on that line. Figures 31a and 31b show C_{NF} plotted along the lifting line for various angles of attack. These diagrams not only represent the variation in C_{NF} along the span, but are also a measure of the load distribution since the wing chord is a constant.

By integrating each of the curves in Figures 31a and 31b and dividing by the length of the diagram the value of C_{NF} may be obtained for the entire wing for each angle of attack represented. These values are plotted together with the force test results for this wing in Figure 32.

Figure 33 gives the longitudinal center of pressure travel versus α for the entire wing. This curve is determined from moment integrations of the C. P. curves in Figures 18–29.

A similar curve for the lateral C. P. travel along the semispan is given in Figure 34. This curve is obtained from moment integrations of the semispan load curves of Figures 31a and 31b.

DISCUSSION

The isometric diagrams of Figures 6–17 furnish a graphic representation of the growth and final collapse of wing surface pressures as the angle of attack is increased. The forward movement of the upper surface boundary layer is shown, beginning with a slight thickening at the

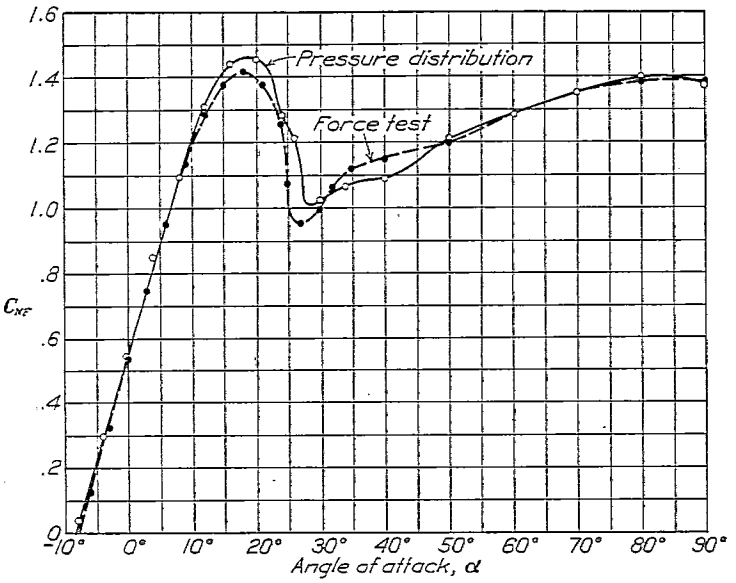

FIG. 32.—Curves of total C_{NF}

trailing edge of the diagram of section 7 at 16° (fig. 10), and culminating in complete flow breakdown for all sections at some angle between 28° and 36°, as shown by the flattening of the upper surface diagrams of Figures 13 and 14. These diagrams indicate the nature of the stresses imposed upon the coverings of rectangular airplane wings in steady flight. Figures 10–13 also

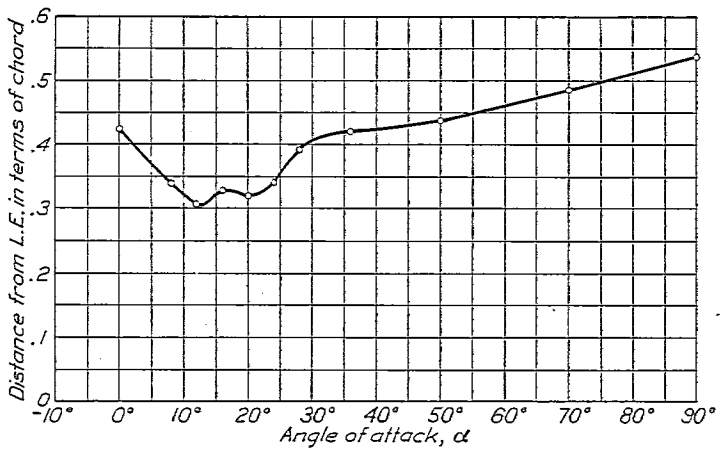

FIG. 33.—Longitudinal center of pressure

show the presence of high nose pressures, signifying that the nose of the Göttingen 387 profile is somewhat too sharp for best results in the vicinity of maximum lift.

The isometric diagrams of Figures 18–29 show the growth and collapse of resultant pressures acting normal to the chord. There is a noteworthy difference both as to shape and size of the pressure diagrams of section 1 as compared with those of other sections. This difference is due to the action of the trailing vortices at the wing tip and practically disappears at 36°. (Fig. 26.)

The curves of longitudinal center of pressure included in Figures 19–29 show that, due to the large tip loads and rearward centers of pressure, undesirable twisting moments are present at the wing tip.

In Figure 30, which contains the curves of C_{NF} for each section, the high loading of the tip section (No. 1) is evident, reaching a maximum value of 2.12 at 26°. The sharp drop from this value to .90 at 34° is indicative of the strong autorotational tendencies of the rectangular wing tip.

In Figures 31a and 31b the excessive tip loads are once more evident. The load distribution departs considerably from the desired elliptical shape which is the theoretical condition for minimum drag. This fact indicates that inaccurate results will be obtained when the theoretical corrections for aspect ratio, biplane interference, and tunnel wall effect are applied to rectangular wings.

In Figure 32, the comparison between pressure distribution and force test values of C_{NF} shows good agreement between $-8°$ and $+10°$ and between 50° and 90°. Between 10° and 50° the discrepancies are variable, reversing in sign at 31°. The results of force tests at large angles

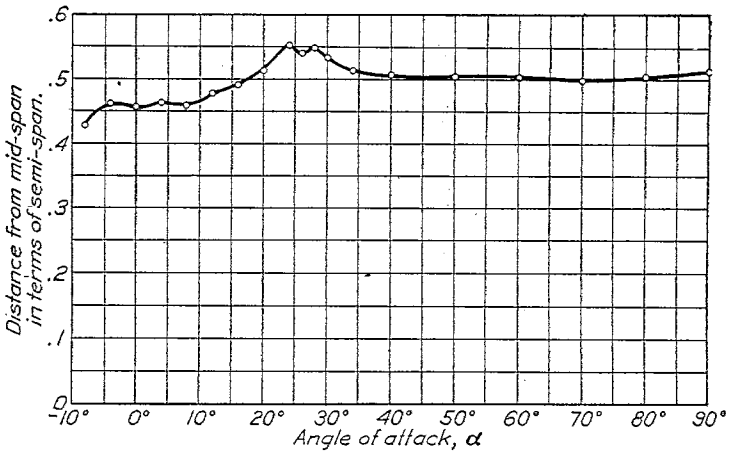

FIG. 34.—Lateral center of pressure

of attack now in progress in the atmospheric tunnel lead to the belief that tunnel wall interference may be the chief cause of these differences. The distance from the wing tip to the tunnel wall was 15 inches for the force tests and about 29 inches for the pressure distribution experiments.

CONCLUSIONS

Although these tests were run at a low Reynolds Number, it is safe to state that a full scale rectangular wing possesses the following disadvantages:

1. The excessively high tip loads up to large angles of attack ($C_{NF}=2.12$ at $\alpha=26°$ for a section 2.48 per cent of semispan from tip) produce large lateral bending moments and longitudinal twisting moments in the wing structure.
2. Above maximum lift such a wing has a high degree of lateral instability.
3. The considerable deviation from elliptical span loading results in increased drag, and also introduces appreciable errors in calculations based on this type of loading.

LANGLEY MEMORIAL AERONAUTICAL LABORATORY,
NATIONAL ADVISORY COMMITTEE FOR AERONAUTICS,
LANGLEY FIELD, VA., *October 27, 1927.*

REFERENCES AND BIBLIOGRAPHY

Reference 1. Reid, Elliott G.: Standardization Tests of N. A. C. A. No. 1 Wind Tunnel. N. A. C. A. Technical Report No. 195 (1924).

2. Norton, F. H., and Bacon, David L.: Pressure Distribution Over Thick Airfoils—Model Tests. N. A. C. A. Technical Report No. 150 (1922).
3. Bacon, David L.: The Distribution of Lift Over Wing Tips and Ailerons. N. A. C. A. Technical Report No. 161 (1923).
4. Reid, Elliott G.: Pressure Distribution Over Thick Tapered Airfoils: N. A. C. A. 81, U. S. A. 27 C Modified, and U. S. A. 35. N. A. C. A. Technical Report No. 229 (1926).
5. Fairbanks, A. J.: Distribution of Pressure Over Model of the Upper Wing and Aileron of a Fokker D–VII Airplane. N. A. C. A. Technical Report No. 254 (1927).
6. Fairbanks, A. J.: Pressure Distribution Tests on PW–9 Wing Models Showing the Effects of Biplane Interference. N. A. C. A. Technical Report No. 271 (1927).